Commun. Comput. Phys.
doi: 10.4208/cicp.180515.230616a

Vol. **21**, No. 2, pp. 423-442
February 2017

An Efficient Implementation of the Divergence Free Constraint in a Discontinuous Galerkin Method for Magnetohydrodynamics on Unstructured Meshes

Christian Klingenberg[1], Frank Pörner[1] and Yinhua Xia[2,*]

[1] *Department of Mathematics, University of Würzburg, Emil-Fischer-Str. 40, 97074 Würzburg, Germany.*
[2] *School of Mathematical Sciences, University of Science and Technology of China, Hefei, Anhui 230026, P.R. China.*

Received 18 May 2015; Accepted (in revised version) 23 June 2016

Abstract. In this paper we consider a discontinuous Galerkin discretization of the ideal magnetohydrodynamics (MHD) equations on unstructured meshes, and the divergence free constraint ($\nabla\cdot\boldsymbol{B}=0$) of its magnetic field $\boldsymbol{B}$. We first present two approaches for maintaining the divergence free constraint, namely the approach of a locally divergence free projection inspired by locally divergence free elements [19], and another approach of the divergence cleaning technique given by Dedner et al. [15]. By combining these two approaches we obtain a efficient method at the almost same numerical cost. Finally, numerical experiments are performed to show the capacity and efficiency of the scheme.

AMS subject classifications: 65M12, 65M20, 65M60, 35L65

Key words: Ideal magnetohydrodynamics equations, discontinuous Galerkin method, divergence free constraint, locally divergence free projection, divergence free cleaning technique.

1 Introduction

Many physical problems arising in a modeling process can be described by the magnetohydrodynamic (MHD) equations which model the dynamics of electrically conducting fluids (e.g. plasma). At high temperature due to ionization, all gases will change to plasma. Therefore the MHD equations are important in many physical applications. Since the equations are highly nonlinear, analytic solutions are not available for the problem. We will focus on the numerical solutions of the ideal MHD equations, represented by an hyperbolic conservation law. Also, an additional involution constraint $\nabla\cdot\boldsymbol{B}=0$ for

*Corresponding author. *Email addresses:* klingen@mathematik.uni-wuerzburg.de (C. Klingenberg), frank.poerner@mathematik.uni-wuerzburg.de (F. Pörner), yhxia@ustc.edu.cn (Y. Xia)

its magnetic field $\boldsymbol{B}$ is needed. Besides the numerical challenges when solving such a nonlinear system, this constraint introduces additional difficulties. On the analytic level the involution constraint is always fulfilled, but numerical experiments indicate that negligence in dealing with the divergence constraint may lead to numerical instability and nonphysical solutions.

Many numerical approaches have been developed to solve conservation laws, e.g. finite volume method (FVM) and finite element method (FEM). Each of them has its advantages and disadvantages. We will focus on the discontinuous Galerkin (DG) method, which combines the flexibility of FEM with the numerical fluxes from FVM. The DG method uses piecewise basis functions which are discontinuous on the boundary of the elements. Normally they are chosen to be piecewise polynomials. Due to the discontinuity of the basis function across cell boundaries, the scheme is very flexible compared to standard continuous finite element method, such as its ability to deal with arbitrary unstructured grids with hanging nodes. Additionally, each cell can have its own polynomial degree independent of its neighbors. Furthermore, the DG scheme admits extremely local data structure (elements only communicate with its immediate neighbors) which leads to high parallel efficiency.

The first discontinuous Galerkin method was introduced by Reed and Hill [28] in 1973. They were interested in the neutron transport problem, i.e. a time independent linear hyperbolic equation. In a series of papers [9–13] Cockburn and Shu developed a framework to solve nonlinear time dependent problems, like Euler or MHD equations. For time integration they are using explicit, nonlinearly stable high order Runge-Kutta time discretizations [30] and for the spatial DG discretization they apply exact or approximate Riemann solvers as interface numerical fluxes. To avoid numerical ascillations near shocks they suggested to apply total variation bounded nonlinear limiters [29]. Due to its good properties, such as high order accuracy and parallel efficiency, the discontinuous Galerkin method has found rapid applications in diverse areas as aeroacoustics, electro-magnetism, gas dynamics and many more. Several numerical results establish the good convergence behavior and reveal an excellent level of details in numerical runs, see e.g. [1].

With regards to the numerical influence of the divergence constraint, several modifications and ideas have been developed to satisfy the constraint or at least reduce the negative impact on the numerical solution. One of the first persons to notice the impact of nonzero divergence to the stability of the numerical schemes were Brackbill and Barnes. In [5], they proposed a global projection method to stabilize their scheme. The projection needs to solve a global elliptic partial differential equation at each time step.

Another approach is given by Powell [25, 27]. The derivation of one-dimensional fluxes (for a finite volume scheme) is based on the symmetrizable form of the MHD equations. In order to symmetrize MHD, we have to add source terms proportional to $\nabla\cdot\boldsymbol{B}$, see [26]. It was discovered later that the robustness of a MHD code can be improved by adding these so called Powell-source term, see [34]. In 2002 Dedner et al. [15] introduced their hyperbolic divergence cleaning technique which has several advantages

over the Powell-source term. They introduced a generalized Lagrangian multiplier to the MHD equations along with some control parameters. While the Powell-source terms only propagates the divergence with the fluid velocity, Dedner's method allows it to control the speed of its movement and additionally smooths the divergence. Both Powell's and Dedner's methods are in general not able to reduce the divergence to zero, like the projection method of Brackbill and Barnes does, but these methods are easily implemented into the DG framework.

In [20, 21] Li et al. introduces a DG scheme which is based on a local reconstruction and preserves the zero divergence of the magnetic field globally. This is done by first discretizing the normal components of the magnetic field along the edges of the elements, followed by a locally divergence free reconstruction inside the elements. Li et al. also introduced in [19] a DG scheme which uses a locally divergence free basis for the magnetic field, which is natural with regard to the DG-formalism.

Another big class of numerical schemes preserving the divergence of the magnetic fields are schemes using constrained transport. The main idea of the constrained transport approach is to use a special discretization of the evolution equation for the magnetic field. It uses a finite volume formalism to evolve the density, momentum, and energy, and exploits Stokes' theorem and uses a face-averaged representation of the magnetic fields to enforce $\nabla \cdot \boldsymbol{B} = 0$ (see [33]).

In this article, we will discuss an implementation of the divergence free constraint on unstructured meshes based on the DG method. Using locally divergence free elements (see [19]) is simple, but it is not trivial to find a basis which results in a well-behaved problem for high polynomial order. Furthermore, we still need to control the global divergence. To achieve this, we first evolve the magnetic field with the standard piecewise polynomial basis, which are not locally divergence free. Then, we project the magnetic field into the subspace of locally divergence free vector fields as a pre-process (*LDFP*). The result does not differ much from the use of locally divergence free elements. And it also decouples the control of the divergence from the Runge-Kutta (RK) step. To control the global part of the divergence, we adopt the approach of Dedner et al. (*DEDNER*). Here we have two parameters to control both the advection speed and the smoothing factor of the divergence. We implement this approach as a post-process procedure. To control both the local and the global part of the divergence we combine both methods (*ProjDED*), where we apply the local projection as a pre-process step, and for the global part we apply the mixed approach of Dedner as a post-process step.

This paper is organized as follows. In Section 2, we introduce the MHD equations along with its involution constraint and the DG-scheme for a two dimensional system of conservation laws. Section 3 is dedicated to the divergence constraint and its numerical treatment. We present the divergence cleaning technique and the locally divergence free basis projection. We combine those two methods to obtain an efficient method *ProjDED* illustrated in Section 4. Subsequently, the numerical verification and experimental validation are discussed with several test problems: accuracy, Orszag-Tang, blast problem and the magnetic rotor. Finally, conclusions are drawn in Section 5.

2 Discontinuous Galerkin method for the MHD equation

2.1 The equations of ideal MHD

The dynamics of electrically conductive fluids is not fully described by the Euler equations. By coupling the Euler equations with Maxwell's equations, we obtain the ideal MHD equations

$$\begin{aligned}
&\partial_t \varrho + \nabla\cdot(\varrho v) = 0,\\
&\partial_t(\varrho v) + \nabla\cdot\left(\varrho v v^T + \left(p+\frac{1}{2}\boldsymbol{B}^T\boldsymbol{B}\right)I - \boldsymbol{B}\boldsymbol{B}^T\right) = 0,\\
&\partial_t \boldsymbol{B} + \nabla\cdot(v\boldsymbol{B}^T - \boldsymbol{B}v^T) = 0,\\
&\partial_t E + \nabla\cdot\left(\left(E+p+\frac{1}{2}\boldsymbol{B}^T\boldsymbol{B}\right)v - (\boldsymbol{B}^T v)\boldsymbol{B}\right) = 0,
\end{aligned} \tag{2.1}$$

together with the involution constraint

$$\nabla\cdot\boldsymbol{B} = 0. \tag{2.2}$$

Here $\varrho, v, \boldsymbol{B}, E$ denotes the density, velocity, magnetic field and total energy, respectively. The MHD equations are closed by connecting the pressure p with the conserved variables

$$p = (\gamma-1)\left(E - \frac{1}{2}\varrho v^T v - \frac{1}{2}\boldsymbol{B}^T\boldsymbol{B}\right).$$

The ratio of specific heats is denoted with $\gamma > 1$. For a derivation of system (2.1) we refer to [32]. If the initial magnetic field satisfies (2.2), the exact solution of system (2.1) will fulfill (2.2) for all time.

2.2 Discontinuous Galerkin finite element method

The discontinuous Galerkin (DG) method is a finite element method (FEM) with discontinuous basis functions which uses the idea of a numerical flux taken from finite volume theory to connect the elements. The DG method has become quite popular for hyperbolic partial differential equations since it combines the flexibility of FEM with the underlying physical dynamics of the equations. We want to refer to the work of Shu and Cockburn [9–14] for a detailed analysis and for the numerical implementation to the book of Hesthaven [18].

Here, we give a brief introduce of the DG method for the following two dimensional conservation laws

$$\frac{\partial \boldsymbol{u}}{\partial t} + \frac{\partial \boldsymbol{f}(\boldsymbol{u})}{\partial x} + \frac{\partial \boldsymbol{g}(\boldsymbol{u})}{\partial y} = 0, \tag{2.3}$$

with the flux functions

$$\boldsymbol{f}(\boldsymbol{u}) = \begin{pmatrix} f_1(\boldsymbol{u}) \\ f_2(\boldsymbol{u}) \end{pmatrix}, \quad \boldsymbol{g}(\boldsymbol{u}) = \begin{pmatrix} g_1(\boldsymbol{u}) \\ g_2(\boldsymbol{u}) \end{pmatrix},$$

where $\boldsymbol{u}=(u_1,u_2)^T$ is in the domain $\Omega\in\mathbb{R}^2$.

Let $\mathcal{T}$ be a regular triangulation of our computational domain Ω with shape-regular elements K, then our test function space is given as

$$V_h=\left\{\boldsymbol{v}=\begin{pmatrix}v_1\\v_2\end{pmatrix}:\ v_i|_K\in P^N(K);\ i=1,2;\ \forall K\in\mathcal{T}\right\},$$

where $P^N(K)$ is the space of polynomial functions of degree at most N over K. Notice that functions in V_h are allowed to be completely discontinuous across element interfaces.

We multiply (2.3) with a test function $\boldsymbol{v}\in V_h$ and integrate over $K\in\mathcal{T}$ to obtain

$$\begin{aligned}0=\int_K \boldsymbol{u}_t\cdot\boldsymbol{v}\,dx-\int_K\left[\begin{pmatrix}f_1(\boldsymbol{u})\\g_1(\boldsymbol{u})\end{pmatrix}\cdot\nabla v_1+\begin{pmatrix}f_2(\boldsymbol{u})\\g_2(\boldsymbol{u})\end{pmatrix}\cdot\nabla v_2\right]dx\\+\int_{\partial K}\left[\Big(\boldsymbol{f}(\boldsymbol{u})n_x+\boldsymbol{g}(\boldsymbol{u})n_y\Big)\cdot\boldsymbol{v}\right]ds,\end{aligned}$$

where $\boldsymbol{n}=(n_x,n_y)^T$ is the outward pointing normal vector of K. We now replace $\boldsymbol{u}$ with the approximate solution $\boldsymbol{u}_h\in V_h$ and the term $\boldsymbol{f}(\boldsymbol{u})n_x+\boldsymbol{g}(\boldsymbol{u})n_y$ by a suitable numerical flux function $\boldsymbol{h}(\boldsymbol{u}_h;\boldsymbol{n})$.

In our simulations, we mainly use the local Lax-Friedrichs flux (LLF). The local Lax-Friedrichs flux along some cell interface with the outer normal $\boldsymbol{n}=(n_x,n_y)^T$ is given by

$$\boldsymbol{h}^{LF}(\boldsymbol{u}_h;\boldsymbol{n}):=\frac{1}{2}\Big(\big(\boldsymbol{f}(\boldsymbol{u}_h^-)+\boldsymbol{f}(\boldsymbol{u}_h^+)\big)n_x+\big(\boldsymbol{g}(\boldsymbol{u}_h^-)+\boldsymbol{g}(\boldsymbol{u}_h^+)\big)n_y\Big)+\frac{\alpha}{2}(\boldsymbol{u}_h^--\boldsymbol{u}_h^+),$$

where a superscript $'-'$ indicates the interior information of the cell and a superscript $'+'$ refers to the exterior information. The constant α is defined as

$$\alpha=\max_{u_h}\left|\lambda\left(\frac{\partial(\boldsymbol{f}n_x+\boldsymbol{g}n_y)}{\partial\boldsymbol{u}_h}\right)\right|.$$

Here $\lambda(\cdot)$ indicates the eigenvalue of the Jacobi matrix, and the maximum is taken over the relevant range of $\boldsymbol{u}_h^{\pm}$.

It is enough to test with basis functions $\boldsymbol{\psi}=(\psi_1,\psi_2)^T\in V_h$ and we end up with the semi-discrete DG formulation for system (2.3) in two space dimensions: Find $\boldsymbol{u}\in V_h$, such that

$$\begin{aligned}\int_K(\boldsymbol{u}_h)_t\cdot\boldsymbol{\psi}\,dx=\int_K\left[\begin{pmatrix}f_1(u_h)\\g_1(u_h)\end{pmatrix}\cdot\nabla\psi_1+\begin{pmatrix}f_2(u_h)\\g_2(u_h)\end{pmatrix}\cdot\nabla\psi_2\right]dx\\-\int_{\partial K}\Big[\boldsymbol{h}(\boldsymbol{u}_h;\boldsymbol{n})\cdot\boldsymbol{\psi}\Big]\,ds,\end{aligned}\tag{2.4}$$

for all basis functions $\boldsymbol{\psi} \in V_h$ and for all $K \in \mathcal{T}$. The extension to more space dimensions and to systems with more than two components is straight forward and is omitted here. In this paper we will focus on two space dimensions, yielding 6 components. The methods can easily extend to three space dimensions. For more details see [18].

By the method of line, we formulate (2.4) as an ODE (for details see e.g. [18])

$$\frac{\partial \bar{\boldsymbol{u}}_h}{\partial t} = \mathcal{L}(\bar{\boldsymbol{u}}_h, t),$$

where $\mathcal{L}$ denotes the right handed side of (2.4) and $\bar{\boldsymbol{u}}_h$ is the coefficient vector of $\boldsymbol{u}_h \in V_h$. To perform a time integration we consider an explicit Runge-Kutta scheme with s stages

$$\begin{cases} \boldsymbol{v}^{(0)} = \bar{\boldsymbol{u}}_h^n, \\ i = 1, \cdots, s\colon \boldsymbol{v}^{(i)} = \sum_{j=0}^{i-1} \alpha_{ij} \boldsymbol{v}^{(j)} + \beta_{ij} \Delta t \mathcal{L}(\boldsymbol{v}^{(j)}, t^n + \gamma_j \Delta t), \\ \bar{\boldsymbol{u}}_h^{n+1} = \boldsymbol{v}^{(s)}. \end{cases} \tag{2.5}$$

To be more precise, we use a strongly stability preserving RK-scheme of order 4 (see [16, 18] for details). The time step is given as (compare to [14])

$$|c| \frac{\Delta t}{h} \leq \frac{\kappa}{(N+1)^2},$$

where $\kappa \in (0,1]$ is a constant. Here h is the minimal diameter of the triangles. The wave speed c is obtained by computing the fast wave arising in the one-dimensional Riemann-Problem located at the interface of each triangle. In our simulations we use $\kappa = 0.2$ independent of the polynomial degree N.

3 Handling the divergence of the magnetic field

A suitable measurement for $\nabla \cdot \boldsymbol{B}$ is given by

$$\|\boldsymbol{B}\|_{\mathrm{div}} := \underbrace{\sum_{K \in \mathcal{T}} \int_K |\nabla \cdot \boldsymbol{B}| \, dx}_{\text{local}} + \underbrace{\sum_{e \in \mathcal{E}} \int_e |[\![\boldsymbol{B}]\!]| \, ds}_{\text{global}}, \tag{3.1}$$

where $\mathcal{E}$ contains all edges of our triangulation $\mathcal{T}$ and $[\![\cdot]\!]$ denotes the jump in the normal component across the edge e. This can either be derived by taking properties of the space $H(\mathrm{div})$ into account [22] or by a functional approach [8]. We see that $\|\boldsymbol{B}\|_{\mathrm{div}}$ consists of two different parts which we want to refer as local and global part. Our first aim is to analyze different techniques and identify whether they operate on the local or on the global part. Second we want to present a scheme which works on both parts.

It is well known that the standard DG-scheme does not preserve a divergence free magnetic field, which is initially divergence free. This is not very surprising since the additional constraint is not used in the derivation of the scheme. Unfortunately the error of the divergence is accumulating in time due to numerical errors and may lead to numerical instabilities. Next we describe some methods that deal with this negative influence.

3.1 Dedner's approach

A well known method is the divergence cleaning given by Dedner et al. [15], where the divergence is coupled with the evolution equation of the magnetic field with a nonphysical variable ψ:

$$\begin{aligned} &\boldsymbol{B}_t+\nabla\cdot(v\boldsymbol{B}^T-Bv^T)+\nabla\psi=0,\\ &\mathcal{D}(\psi)+\nabla\cdot\boldsymbol{B}=0, \end{aligned} \tag{3.2}$$

and $\mathcal{D}$ is a linear differential operator. One possible choice is the hyperbolic approach $\mathcal{D}(\psi)=\frac{1}{c_h^2}\partial_t\psi$ where ψ satisfies the wave equation

$$\partial_{tt}^2\psi-c_h^2\Delta\psi=0.$$

If we choose the parabolic approach $\mathcal{D}(\psi)=\frac{1}{c_p^2}\psi$, we obtain that ψ satisfies the heat equation

$$\psi_t-c_p^2\Delta\psi=0.$$

Combing both yields the mixed approach $\mathcal{D}(\psi)=\frac{1}{c_h^2}\partial_t\psi+\frac{1}{c_p^2}\psi$ where ψ satisfies the telegraph equation

$$\partial_{tt}^2\psi+\frac{c_h^2}{c_p^2}\partial_t\psi-c_h^2\Delta\psi=0. \tag{3.3}$$

The variable ψ can be seen as an abstract measurement for $\nabla\cdot\boldsymbol{B}$. For the parabolic approach we obtain

$$\psi(\boldsymbol{x},t)=-c_p^2\nabla\cdot\boldsymbol{B}(\boldsymbol{x},t),$$

and for the hyperbolic approach we obtain for $\psi_0(\boldsymbol{x}):=\nabla\cdot\boldsymbol{B}(\boldsymbol{x},0)$

$$\psi(\boldsymbol{x},t)=-c_h^2\int_0^t\nabla\cdot\boldsymbol{B}(\boldsymbol{x},\tau)\,d\tau+\psi_0(\boldsymbol{x}).$$

For the mixed approach an analytic solution is not possible. Based on the parabolic and hyperbolic approach and by our assumption $\nabla\cdot\boldsymbol{B}(\boldsymbol{x},0)=0$, we initialize $\psi(\boldsymbol{x},0)=0$.

The parameter $c_h\in(0,\infty)$ influences the advection speed, at which the error in the divergence is transported to the boundary of the domain. And the parameter $c_p\in(0,\infty)$

controls the smoothing effect of the parabolic approach. For more details see [15] and for possible choices of c_h,c_p see Altmann [1]. We choose in our simulations $c_h = 7c_v$. To compute c_v, we first compute the speeds c_i of the fast waves arising on the boundaries of each cell. Then set $c_v = \max_i c_i$. Our aim is to choose c_h faster than the maximum wave speed of system (2.1), to have the divergence transported fast enough to the boundary.

To determine c_p we follow the suggestion in [15] and take the ratio between hyperbolic and parabolic effects to be constant

$$c_r = \frac{c_p^2}{c_h} \in (0,\infty).$$

It is found by Dedner that this choice gives results which are quite independent of the grid resolution and the scheme used. Furthermore they suggested the value $c_r = 0.18$, which is a good compromise between damping and hyperbolic transport. If more damping is forced, we lose the effect of the hyperbolic transport of the error in the divergence (see [1]). For the one-dimensional MHD system and under some simplifying assumptions, Dedner proved that $\nabla\cdot\boldsymbol{B}$ gets transported out of the domain when the hyperbolic approach is used. If the parabolic approach is used, we obtain a smoothing on $\nabla\cdot\boldsymbol{B}$. For the mixed approach both properties are obtained. This method is also very effective in more than one space dimension.

We solve the system (3.2) in an operator split approach. First, we evolve the magnetic equation $\boldsymbol{B}_t + \nabla\cdot(v\boldsymbol{B}^T - Bv^T) = 0$ in (2.1). It follows by solving the system of Dedner's hyperbolic approach

$$\begin{aligned} &\boldsymbol{B}_t + \nabla\psi = 0, \\ &\partial_t\psi + c_h^2\nabla\cdot\boldsymbol{B} = 0, \end{aligned} \tag{3.4}$$

with a DG scheme. We apply the DG formalism to (3.4) with the Riemann solver suggested in [15]. In the computation of the Riemann solver for (3.4), we need the value of ψ and $\boldsymbol{B}\cdot\boldsymbol{n}$ at both sides of the cell boundary. Therefore, the hyperbolic divergence cleaning works on the global part of our measurement of the divergence.

If we want to use the mixed approach, we have to take the parabolic source term from the equation (3.3) into account. Again, in the operator splitting approach we only need to solve the additional ordinary differential equation

$$\partial_t\psi = -\frac{c_h^2}{c_p^2}\psi.$$

This can be done exactly

$$\psi^{n+1} = \exp\left(-\Delta t_n \frac{c_h^2}{c_p^2}\right)\psi^{n^*}. \tag{3.5}$$

where ψ^{n^*} is the solution to system (3.4).

For the hyperbolic approach, it can be shown (see [15]) that $\nabla\cdot\boldsymbol{B}$ gets transported to the boundary. For the parabolic approach, the damping is forced on $\nabla\cdot\boldsymbol{B}$, hence this approach works on the local part of $\nabla\cdot\boldsymbol{B}$. We see that the mixed approach operates on the local and on the global part of the divergence. An overview of the implementation is shown in Algorithm 1.

3.2 Locally divergence free basis

To deal with the local part, another possibility is to modify the test function space V_h to guarantee that the numerical solution is locally divergence free. Hence use

$$V_h^*:=\Big\{\boldsymbol{v}\in\big(L^2(\Omega)\big)^6:\ \boldsymbol{v}|_K\in\Big(P^N(K)\Big)^6\wedge\nabla\cdot(v_4,v_5)|_K=0,\ \forall K\in\mathcal{T}\Big\},$$

where v_4 and v_5 denote the x and y component of the two dimensional magnetic field respectively. For MHD such an approach is made in [19].

To construct a basis of V_h^* we define the test-function space for the magnetic field

$$\mathrm{LDF}^N(K):=\Big\{\boldsymbol{p}\in\Big(P^N(K)\Big)^2:\ \nabla\cdot\boldsymbol{p}=0\Big\}.$$

In the following we will show, that it is not easy to find a suitable basis of V_h^*. First we will concentrate on finding a basis of the space $LDF^N(K)$.

Lemma 3.1. *The dimension of the space $LDF^N(K)$ is given by $\frac{1}{2}(N+2)(N+3)-1$. Furthermore a basis of $LDF^N(K)$ can be obtained by taking the curl of basis function of the space $P^{N+1}(K)$.*

A proof can be found in [19] or [6]. This allows us to construct a basis, e.g. if we take the curl of the monomial basis of $P^{N+1}(K)$. To avoid the poor condition of the resulting mass-matrix (Fig. 1), we take the Gauss-Lobatto points into account, to hopefully adapt the stability and approximation property of the Lagrange polynomials.

Denote $\{p_1,\cdots,p_s\}$ the Gauss-Lobatto points of order $N+1$ in the element K. Let $gl_i\in P^{N+1}(K)$ the unique functions satisfying

$$gl_i(p_j)=\delta_{ij},\quad\forall i,j=1,\cdots,s.$$

By Lemma 3.1, the set

$$GL^N(K):=\{\nabla\times gl_1,\cdots,\nabla\times gl_{s-1}\}$$

is a basis of $LDF^N(K)$. In our simulations we observed that this basis yields good approximation results and at the same time an acceptable condition for the mass matrix, see Fig. 1. Note that this method (we will refer to it as *LDFB*, see Fig. 2) only controls the local part of the divergence. This is due to the fact, that the basis functions are chosen independent from the neighbouring cells.

In addition, it could be easy to implement a projection step into an existing code, than to change the underlying basis functions $\big(P^N(K)\big)^2$. Therefore, we use a local L^2

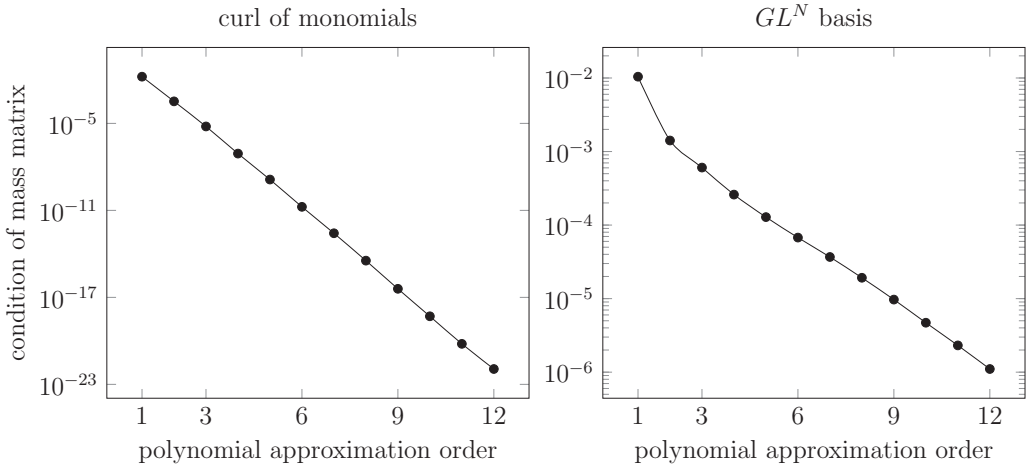

Figure 1: Reciprocal condition number for the mass matrix for two different bases of $LDF^N(K)$ on a reference triangle.

projection from $\left(P^N(K)\right)^2$ to $\mathrm{LDF}^N(K)$ instead of changing the basis, which can be done nearly without additional numerical expense. Note that the projection is decoupled from the DG-discretization. Thus we can use the basis by applying Gram-Schmidt procedure to the monomial basis of $LDF^N(K)$. First let P_K be the L^2 projection in the element K,

$$P_K : \left(P^N(K)\right)^2 \to \mathrm{LDF}^N(K)$$

Now define the local operator $P_K^{\mathrm{ldf}} : \left(P^N(K)\right)^8 \to \left(P^N(K)\right)^8$ through

$$\boldsymbol{q} = P_K^{\mathrm{ldf}}(\boldsymbol{p}) : \Longleftrightarrow q_i = p_i,\ i \neq 4,5 \text{ and } (q_4, q_5) = P_K((p_4, p_5)).$$

The global operator $P_{\mathrm{ldf}} : V_h \to V_h^*$ is now defined

$$\boldsymbol{q} = P_{\mathrm{ldf}}(\boldsymbol{p}) : \Longleftrightarrow \boldsymbol{q}|_K = P_K^{\mathrm{ldf}}(\boldsymbol{p}|_K),\ \forall K \in \mathcal{T}.$$

In Fig. 3 we compare two different approaches. In the first approach (*LDFB*), we adopt the test function space V_h^* in the DG-discretization. In the second approach (*LDFP*), we use V_h as test function space and applying P_{ldf} every time before computing the Runge-Kutta step. The results do not differ much. We therefore suggest a hybridized method *ProjDED* presented in Fig. 2. Also a comparison between the different methods is provided in Fig. 2. For the description of the other schemes see Section 4.

In the hybridized method *ProjDED*, the projection is applied before the RK-step in order to work as a pre-smoother for the divergence. Dedner's mixed approach is used as a post-process to deal with the global part of the divergence and the additional local error introduced by the RK-step. Since the operator P_K is a projection between finite dimensional spaces the numerical for applying P_{ldf} cost are negligible (see also Table 2).

In the following lemma we show that the projection is compatible with a positivity preserving method, as long as we use positivity preserving limiter.

Lemma 3.2. *Let $q=(\varrho,\boldsymbol{v},\boldsymbol{B},E)\in(L^2(K))^6$ such that $\varrho>0$ and $p>0$ holds. Then the operator P_{ldf} defined above preserves positivity of the density and pressure in the means, meaning for*

$$\tilde{q}:=(\tilde{\varrho},\tilde{\boldsymbol{v}},\tilde{\boldsymbol{B}},\tilde{E}):=P_{ldf}(q)$$

we obtain

$$\int_K \tilde{p}\,dx>0 \quad \textit{and} \quad \int_K \tilde{\varrho}\,dx>0.$$

Proof. With $\|P_K\|\leq 1$ we obtain $\|\tilde{B}\|_K\leq\|B\|_K$. Hence, we get the positivity of the pressure in the mean

$$\begin{aligned}\int_K \tilde{p}\,dx &= \int_K (\gamma-1)(E-\frac{1}{2}\varrho v^2-\frac{1}{2}\tilde{B}^2)\,dx\\ &\geq \int_K (\gamma-1)(E-\frac{1}{2}\varrho v^2-\frac{1}{2}B^2)\,dx\\ &= \int_K p\,dx>0.\end{aligned}$$

Meanwhile, the density is not changed by P_{ldf}, yielding $\tilde{\varrho}=\varrho$. □

Remark 3.1. Lemma 3.2 shows that the projection can be included into an existing positivity preserving scheme, as long as a positivity preserving limiter is applied after each projection. Here we refer the reader to the results obtained for MHD-DG given by Li [7]. For some positivity preserving limiter we refer to [31,35].

4 Details of the implementation

The aim of this chapter is to give some insight into our implementation. The step to compute the solution at the next time level is divided into three levels: The pre-process level, the DG-Runge-Kutta step and a post-process level. In the pre- and post-process level we apply some methods to deal with the error in the divergence. We only describe the *ProjDED* method, since the others can be described similar. Due to the operator splitting approach for *DEDNER* the value ψ is treated after we performed a DG-discretization to (2.1), so it behaves like a post-processing operation.

Initialize

$$\begin{aligned} \boldsymbol{q}_h^0 &:= \begin{pmatrix} \varrho_h^0 & \boldsymbol{v}_h^0 & \boldsymbol{B}_h^0 & E_h^0 \end{pmatrix} \in V_h \\ \psi_h^0 &:= 0 \\ k &:= 0 \end{aligned}$$

while *Breaking condition is not satisfied* **do**

pre-process

$$\boldsymbol{q}_h^{k+1/3} := P_{ldf}(\boldsymbol{q}_h^k)$$

DG-Runge-Kutta

Determine Δt^k and apply SSP-RK of order 4 with initial data $\boldsymbol{q}_h^{k+1/3}$ to the DG discretization (LLF flux) of the MHD equations (2.1) and obtain $\boldsymbol{q}_h^{k+2/3}$

post-process

Apply SSP-RK of order 4 with initial data $\boldsymbol{B}_h^{k+2/3}$ and ψ_h^k to the DG discretization (flux given in [15]) of the system

$$\begin{aligned} \boldsymbol{B}_t + \nabla \psi &= 0 \\ \partial_t \psi + c_h^2 \nabla \cdot \boldsymbol{B} &= 0 \end{aligned}$$

to obtain $\boldsymbol{B}_h^{k+1}$ and $\psi_h^{k+1/2}$. Now apply operator splitting for the source term coming from the parabolic approach

$$\psi_h^{k+1} := \exp\left(-\frac{c_h^2}{c_p^2} \Delta t^k \right) \psi_h^{k+1/2}$$

Set $\boldsymbol{q}_h^{k+1} := \begin{pmatrix} \varrho_h^{k+2/3} & \boldsymbol{v}_h^{k+2/3} & \boldsymbol{B}_h^{k+1} & E_h^{k+2/3} \end{pmatrix}$

Set $k \mapsto k+1$

end

Algorithm 1: *ProjDED*. For clarity we dropped the use of a limiter.

5 Numerical experiments

The schemes we are using in the numerical tests are the following. The *BASE* scheme is just the DG scheme with test function space V_h. The *LDFB* (locally divergence free basis) scheme is the DG scheme with the test function space V_h^*. If we use instead a locally divergence free projection as a pre-process step for the BASE scheme, we call the scheme *LDFP*. In the *DEDNER* scheme, the mixed approach of Dedner is applied. The implementation is given similar as in algorithm 1. Hence we interpret it as a post-process method. And *ProjDED* is the combined method of LDFP and DEDNER described above (see Fig. 2 and Algorithm 1). Unless otherwise stated the local Lax-Friedrichs (LLF) flux is used.

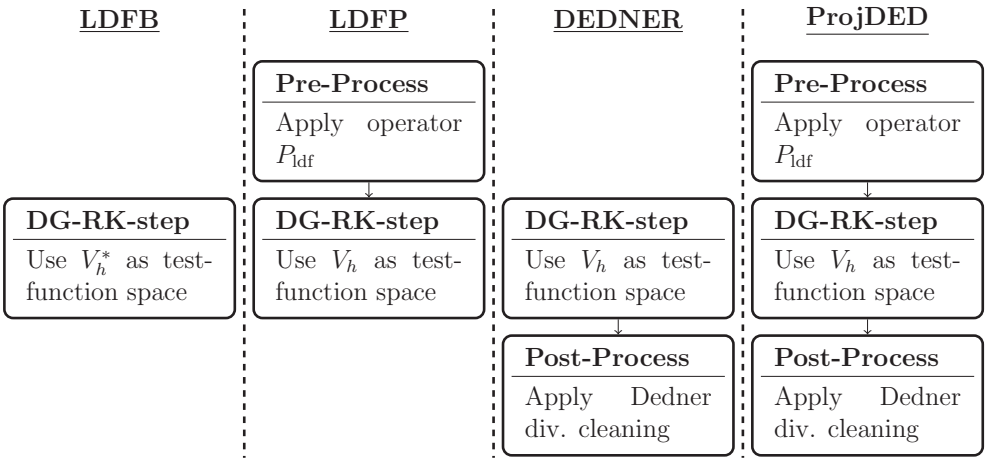

Figure 2: Overview over the different schemes used. We separate each DG-RK step into a pre-process step, the actual DG-RK-step and a post-process step.

To show the impact of the divergence, we compute the numerical convergence rates for the genuinely two dimensional vortex problem given in [19, Section 3.2.1]. We only give the results for the density in Table 1, since for the other components the results look the same. We see that the error in the divergence decreases significantly the numerical order of convergence. It can be seen that our hybrid method is not destroying the numerical convergence order. Furthermore we encounter a strange behavior of our convergence order. For even polynomial order we get order $N+1/2$ but for uneven polynomial order we obtain the optimal rate of $N+1$. In the hydrodynamic case we do not discover such a behavior. The different behavior of the L^2-rate of convergence for even and uneven polynomial approximations was also discovered in [17] and [23].

If we take a look at the computational time needed for the local projection method we define one complete time-step in the 4th order SSP-RK without any modifications to be 100%. In Table 2 we compare the time needed for one projection step compared with one step in the SSP-RK.

Table 1: Numerical order of convergence for the density of the vortex problem.

ϱ	**N=1**									
scheme	BASE		LDFB		LDFP		DEDNER		ProjDED	
h/h_0	L^2-error	order	L^2-error	order	L^2-error	order	L^2-error	order	L^2-error	order
2^{-3}	8.1e-03		8.5e-03		7.5e-03		7.8e-03		8.0e-03	
2^{-4}	4.7e-03	0.78	5.5e-03	0.64	4.9e-03	0.62	5.8e-03	0.42	6.3e-03	0.34
2^{-5}	1.6e-03	1.55	1.9e-03	1.49	1.6e-03	1.59	2.1e-03	1.50	2.3e-03	1.47
2^{-6}	4.1e-04	1.99	4.0e-04	2.27	4.0e-04	2.02	4.6e-04	2.16	4.9e-04	2.22
	N=2									
2^{-3}	7.8e-03		7.9e-03		7.4e-03		7.3e-03		7.4e-03	
2^{-4}	2.7e-03	1.53	2.0e-03	2.00	2.0e-03	1.91	1.7e-03	2.07	1.7e-03	2.09
2^{-5}	6.0e-04	2.16	4.0e-04	2.31	4.3e-04	2.18	3.6e-04	2.26	3.6e-04	2.26
2^{-6}	1.0e-04	2.57	7.5e-05	2.41	7.6e-04	2.52	6.2e-05	2.55	6.2e-05	2.55
	N=3									
2^{-3}	3.0e-03		2.2e-03		2.4e-03		2.4e-03		2.4e-03	
2^{-4}	3.4e-04	3.15	1.5e-04	3.86	1.5e-04	3.97	1.4e-04	4.12	1.4e-04	4.11
2^{-5}	3.1e-05	3.43	1.0e-05	3.89	9.5e-06	4.02	7.0e-06	4.31	7.1e-06	4.30
2^{-6}	2.7e-06	3.54	6.4e-07	3.96	6.0e-07	3.98	4.1e-07	4.11	4.2e-07	4.09
	N=4									
2^{-3}	5.6e-04		3.8e-04		3.8e-04		3.7e-04		3.7e-04	
2^{-4}	4.2e-05	3.75	1.4e-05	4.79	1.4e-05	4.78	1.3e-05	4.86	1.3e-05	4.87
2^{-5}	3.4e-06	3.58	5.9e-07	4.56	5.9e-07	4.56	5.6e-07	4.51	5.6e-07	4.51
2^{-6}	3.0e-07	3.51	2.7e-08	4.52	2.6e-08	4.48	2.5e-08	4.49	2.5e-08	4.50

Table 2: Computational time needed for one projection step in relation to one time-step with 4th order SSP-RK for different mesh sizes and polynomial orders.

grid size	8x8	16x16	32x32	64x64	128x128
N=1	3.7%	1.8%	1.1%	0.4%	0.2%
N=2	3.2%	1.6%	1.0%	0.3%	0.2%
N=3	2.0%	1.5%	0.7%	0.2%	0.2%
N=4	2.0%	1.5%	0.5%	0.2%	0.2%
N=5	2.0%	1.4%	0.5%	0.2%	0.3%
N=6	2.1%	1.4%	0.4%	0.3%	0.3%
N=7	2.0%	1.3%	0.3%	0.3%	0.3%
N=8	2.0%	1.1%	0.3%	0.3%	0.3%

We furthermore test our numerical scheme with 3 different test problems: Orszag-Tang [24], blast problem [2] and the magnetic rotor [33]. We observed that *ProjDED* runs stable and the results are in good agreement with results given in the literature. In Figs. 4-6, we compare the divergence $\|B\|_{\text{div}}$ for different numerical methods for this problems.

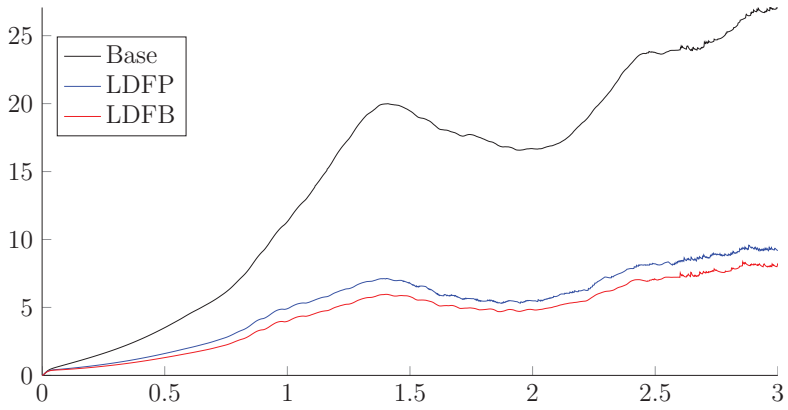

Figure 3: Measurement of the divergence for Orszag-Tang vortex problem. The results of LFDB and LDFP do not differ much.

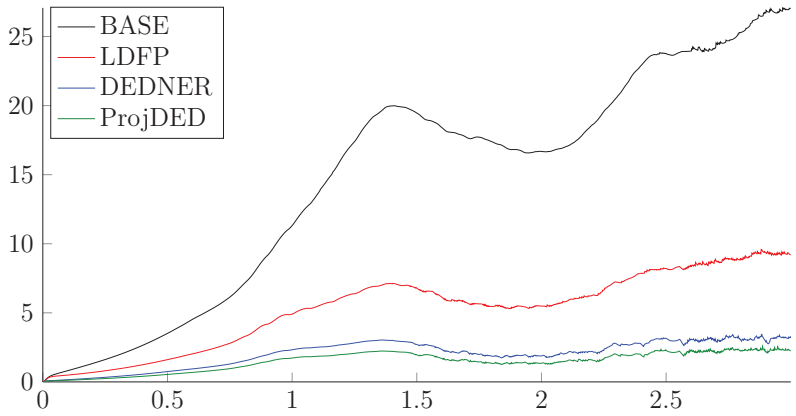

Figure 4: Divergence error for different schemes for the Orszag-Tang vortex problem

The combined method *ProjDED* gives good result in these tests. In the computation, 80.000 triangles are used.

To show the difference between the scheme *DEDNER* and *ProjDED*, we also plot the relative error

$$\frac{\mathrm{div}(DEDNER)-\mathrm{div}(ProjDED)}{\mathrm{div}(DEDNER)}, \tag{5.1}$$

where $\mathrm{div}(DEDNER)$ denotes $\|\boldsymbol{B}\|_{\mathrm{div}}$ when the algorithm *DEDNER* is used. The results are given in Fig. 7 and we see that *ProjDED* is about 25% more efficient than the Dedner scheme in our test simulations. Note that both schemes have almost the same numerical effort.

We also tested the 3-wave solver as a numerical flux specially designed for MHD by Klingenberg [3, 4]. This flux takes the divergence constraint into account. We expect for the combination of the 3-wave solver and our hybrid method *ProjDED* an improvement

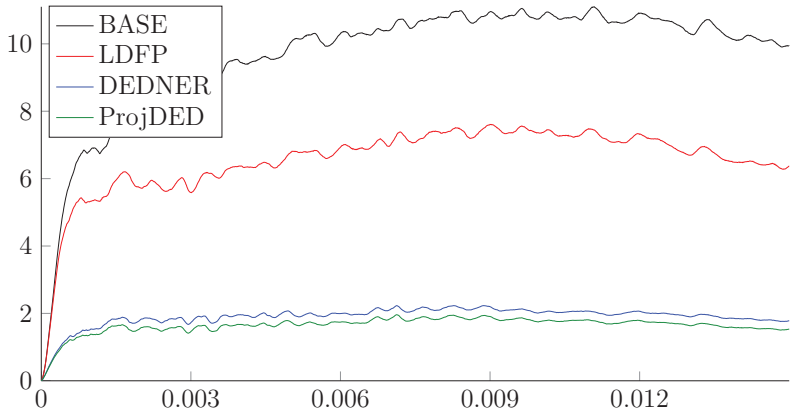

Figure 5: Divergence error for different schemes for the blast problem

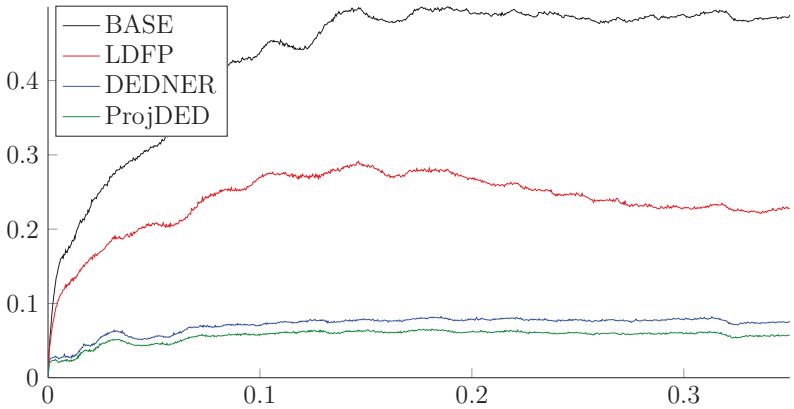

Figure 6: Divergence error for different schemes for the magnetic rotor problem

in our numerical scheme both in resolution of details for long time simulations and a decrease in the divergence compared to LLF. Both results are confirmed – see Fig. 8.

6 Conclusion

We have presented four methods to deal with the error of the divergence of the magnetic field and compared their efficiency on several test problems. The advantage of *LDFB* is that the resulting magnetic field is locally divergence free for all time. This is guaranteed by the scheme itself, we do not need any pre- or post-process operators.

In *LDFP*, we project the magnetic field into the subspace of locally divergence free vector fields. The results do not differ from those obtained by *LDFB* and we have decoupled the control of the divergence from the RK-step. In fact, if we use the projection before each stage in the RK-step, both schemes yield almost the same results.

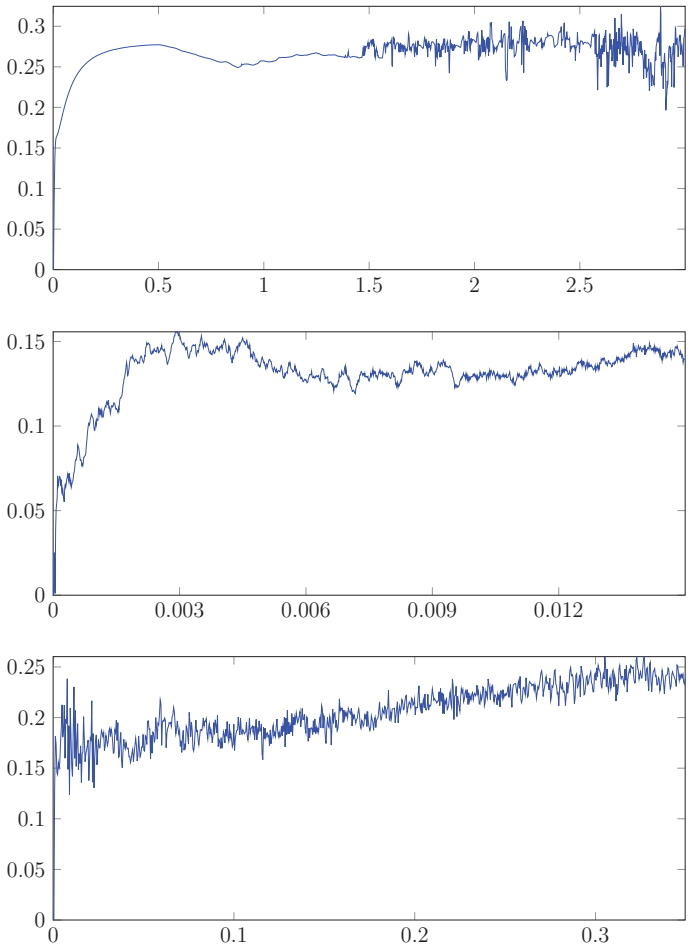

Figure 7: Relative error (5.1) for different test problems. Top: Orszag-Tang vortex problem, Middle: Blast problem, Bottom: Magnetic rotor

Note that *LDFB* and *LDFP* only control the local part of the divergence. This is due to the fact that the basis functions are chosen independently from the neighbouring cells. A very effective way of controlling the global error in the divergence is the approach of Dedner et al. (*DEDNER*), where we have two parameters to control both the advection speed and the smoothing factor of the divergence, but choosing these parameters is not trivial.

To control both the local and the global part of the divergence, we developed the scheme *ProjDED* as a combination of the local projection as a pre-process step, and the mixed approach of Dedner et al. as a post-process step. If the numerical method used is positivity preserving, the combination of the projection is still positivity preserving. Thus, the projection does not introduce additional instabilities regarding positivity.

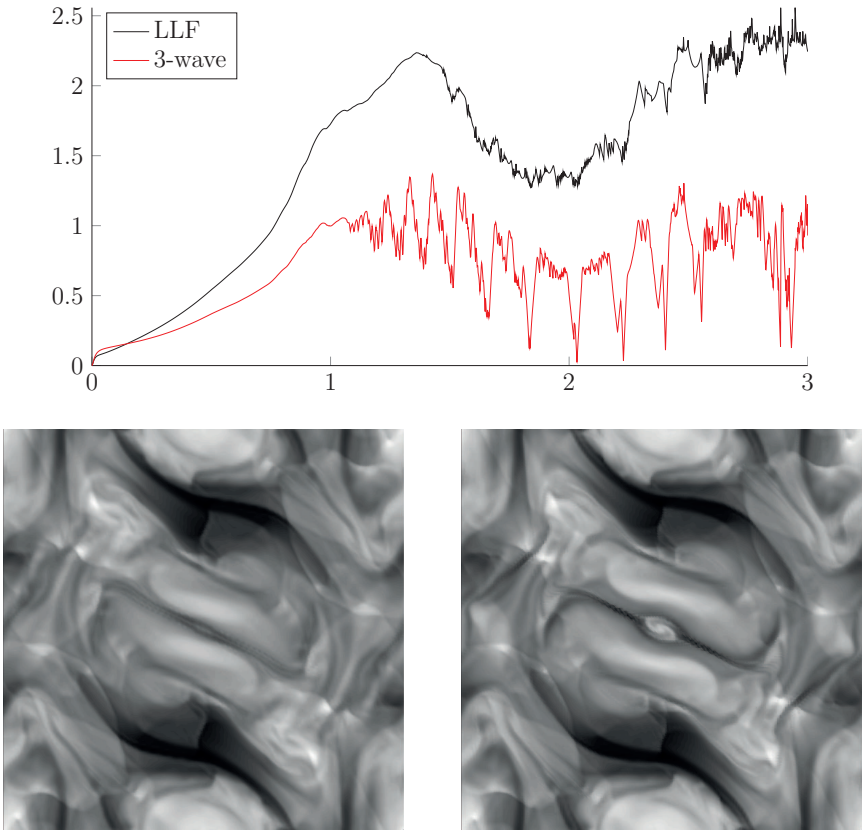

Figure 8: Demonstration of the impact of different numerical fluxes both on the level of resolution for long time computations and on the divergence. Top: $\|B\|_{\text{div}}$ for the LLF-flux and for the 3-wave solver. Bottom: Grayscale image of the density of Orszag-Tang vortex problem at time $t=6$ with different numerical flux functions. Left: local Lax-Friedrichs, Right: 3-wave solver. Both computations are done on 45.000 triangles with linear polynomials, TVB-limiter and LDFP.

We see that all of these methods stabilize the DG method in the sense that the error in the divergence stays small or at least is significant smaller than the solution of *BASE*. As a result, we avoid non-physical oscillations leading to a more stable scheme. If we look at the relation of computational costs and efficiency, *LDFP* clearly wins. But since we are interested in getting $\nabla\cdot\boldsymbol{B}$ close to zero, it is worth to implement *DEDNER*. As already mentioned, the numerical costs of *LDFP* are negligible. *ProjDED* is as costly as the Dedner approach. As a result we conclude that *ProjDED* is a suitable and robust method to deal with the negative influence of a non-vanishing divergence of the magnetic field.

Acknowledgments

Research of Y. Xia is supported by the NSFC grants No.11371342, No. 11471306.

References

[1] C. Altmann. *Explicit Discontinuous Galerkin Methods for Magnetohydrodynamics*. PhD thesis, University of Suttgart, 2012.

[2] D.S. Balsara and D.S. Spicer. A staggered mesh algorithm using high order godunov fluxes to ensure solenoidal magnetic fields in magnetohydrodynamic simulations. *Journal of Computational Physics*, 149:270–292, 1999.

[3] F. Bouchut, C. Klingenberg, and K. Waagan. A multiwave approximate rieman solver for ideal mhd based on relaxation. i: theoretical framework. *Numerische Mathematik*, 108:7–42, 2007.

[4] F. Bouchut, C. Klingenberg, and K. Waagan. A multiwave approximate rieman solver for ideal mhd based on relaxation. ii: numerical implementation with 3 and 5 waves. *Numerische Mathematik*, 115:647–679, 2010.

[5] J. U. Brackbill and D.C. Barnes. The effect of nonzero $\nabla \cdot b$ on the numerical solution of the magnetohydrodynamic equations. *Journal of Computational Physics*, 35:426–430, 1980.

[6] F. Brezzi, J. Douglas, and L.D. Marini. Two families of mixed finite elements for second order elliptic problems. *Numerical Mathematics*, 47:217–235, 1985.

[7] Y. Cheng, F. Li, J. Qiu, and L. Xu. Positivity-preserving dg and central dg methods for ideal mhd equations. *Journal of Computational Physics*, 238:255–280, 2013.

[8] B. Cockburn, F. Li, and C.-W. Shu. Locally divergence-free discontinuous galerkin methods for the maxwell equations. *Journal of Computational Physics*, 194:588–610, 2003.

[9] B. Cockburn and C.-W. Shu. Tvb runge-kutta local projection discontinuous galerkin finite element method for conservation laws ii: general framework. *Mathematics of Computation*, 52:411–435, 1989.

[10] B. Cockburn and C.-W. Shu. Tvb runge-kutta local projection discontinuous galerkin finite element method for conservation laws iii: One-dimensional systems. *Journal of Computational Physics*, 84:90–113, 1989.

[11] B. Cockburn and C.-W. Shu. The runge-kutta local projection discontinuous galerkin finite element method for conservation laws iv: The multidimensional case. *Mathematics of Computation*, 54:545–581, 1990.

[12] B. Cockburn and C.-W. Shu. The runge-kutta local projection p^1-discontinuous-galerkin finite element method for scalar conservation laws. *Mathematical Modelling and Numerical Analysis*, 25:337–361, 1991.

[13] B. Cockburn and C.-W. Shu. The runge-kutta discontinuous galerkin method for conservation laws v: Multidimensional systems. *Journal of Computational Physics*, 141:199–224, 1997.

[14] B. Cockburn and C.-W. Shu. Runge-kutta discontinuous galerkin methods for convection-dominated problems. *Journal of Scientific Computing*, 16:173–261, 2001.

[15] A. Dedner, F. Kemm, D. Kroener, T. Schnitzer C.-D. Munz, and M. Wesenberg. Hyperbolic divergence cleaning for the mhd equations. *Journal of Computational Physics*, 175:645–673, 2002.

[16] S. Gottlieb, C.-W. Shu, and E. Tadmor. Strong stability preserving high order time discretization method. *SIAM Rev.*, 43:89–112, 2001.

[17] J. Guzmán and B. Rivière. Sub-optimal convergence of non-symmetric discontinuous galerkin methods for odd polynomial approximations. *J. Sci. Comp.*, 40:273–280, 2009.

[18] J. S. Hesthaven and T. Warburton. *Nodal Discontinuous Galerkin Methods*. Springer Verlag, 2008.

[19] F. Li and C.-W. Shu. Locally divergence-free discontinuous galerkin methods for mhd equa-

tions. *Journal of Scientific Computing*, 22-23:413–442, 2005.
[20] F. Li and L. Xu. Arbitrary order exactly divergence-free central discontinuous galerkin methods for ideal mhd equations. *Journal of Computational Physics*, 231:2655–2675, 2012.
[21] F. Li, L. Xu, and S. Yakovlev. Central discontinuous galerkin methods for ideal mhd equations with the exactly divergence-free magnetic field. *Journal of Computational Physics*, 230:4828–4847, 2011.
[22] J.C. Nédélec. A new family of mixed finite elements in r3. *Numerical Mathematics*, 50:57–81, 1986.
[23] J. T. Oden, I. Babuska, and C. E. Baumann. A discontinuous hp finite element method for diffusion problems. *Journal of Computational Physics*, 146:491–519, 1998.
[24] S. Orszag and C.-M. Tang. Small-scale structure of two-dimensional magnetohydrodynamic turbulence. *Journal of Fluid Mechanics*, 90:129–143, 1979.
[25] K. G. Powell. An approximate riemann solver for magnetohydrodynamics (that works in more than one dimension). *ICASE-Report*, 94-24, 1994.
[26] K. G. Powell, P. L. Row, R. S. Myong, T. Gombosi, and D. De Zeeuw. The symmetric form of magnetohydrodynamics equation. *Numer. Methods Mech. Contin. Media*, 1:26, 1994.
[27] K. G. Powell, P. L. Row, R. S. Myong, T. Gombosi, and D. De Zeeuw. An upwind scheme for magnetohydrodynamics. *Numerical Methods for Fluid Dynamics*, V:163, 1994.
[28] W. H. Reed and T. R. Hill. Triangular mesh methods for the neutron transport equation. *Tech. Report LA-UR-73-479, Los Alamos Scientific Laboratory*, 1973.
[29] C.-W. Shu. Tvb uniformly high-order schemes for conservation laws. *Mathematics of Computation*, 49:105–121, 1987.
[30] C.-W. Shu and S. Osher. Efficient implementation of essentially non-oscillatory shoch-capturing schemes. *Journal of Computational Physics*, 77:439–471, 1988.
[31] C.-W. Shu and X. Zhang. On positivity-preserving high order discontinuous galerkin schemes for compressible euler equations on rectangular meshes. *Journal of Computational Physics*, 229:8918–8934, 2010.
[32] M. Torrilhon. *Zur Numerik der idealen Magnetohydrodynamik*. PhD thesis, Eidgenssische Technische Hochschule Zrich, 2003.
[33] G. Tóth. The $\nabla \cdot b = 0$ constraint in shock-capturing magnetohydrodynamics codes. *Journal of Computational Physics*, 161:605, 2000.
[34] K. Waagan, C. Klingenberg, and C. Federrath. A robust numerical scheme for highly compressible magnetohydrodynamics: Nonlinear stability, implementation and tests. *Journal of Computational Physics*, 230:3331–3351, 2011.
[35] X. Zhang, Y. Xia, and C.-W. Shu. Maximum-principle-satisfying and positivity-preserving high order discontinuous galerkin schemes for conservation laws on triangular meshes. *Journal of Scientific Computing*, 50(1):29–62, 2012.